ACTIVE FILTERS

An electrical filter may be defined as "a transducer for separating waves on the basis of their frequencies" (1). There are numerous everyday uses for such devices ranging from the filter that allows one to select a particular radio station, to the circuit that detects brainwaves, to resonant cavities that operate at microwave frequencies. Indeed, filters are needed for operation across the electromagnetic spectrum. Furthermore, they are required to perform frequency selection to satisfy various specialized approximating functions, not necessarily confined to the conventional low-pass, bandpass, high-pass, and band-stop forms.

However, the purpose of this article is to focus on a particular category of filter, the active filter, whose evolution over the past 40 years has been heavily influenced by advances in microelectronic circuit fabrication. The earliest active filters were motivated by the need to overcome significant limitations of inductor–capacitor (LC) passive filters, namely:

1. In the audio band, inductors are bulky and prone to pick up.
2. Resistor–capacitor (RC) filter structures offer a limited range of responses and are subject to substantial passband attenuation.

By contrast, active RC structures can realize (theoretically) lossless filter characteristics in miniaturized form. Passive and active filter properties are summarized in Table 1.

A disadvantage of the active filter is its need for a power supply and the incorporation of one or more active elements, usually operational amplifiers. As a result, highly selective filters need careful design so as to avoid instability. However, as active filter design has matured, a small number of highly reliable topologies have evolved that provide solid performance across a variety of fabrication technologies.

The earliest active filters used discrete components and were based upon direct synthesis of RC sections with appropriately embedded active devices such as the negative impedance converter (2). Second-order sections were then cascaded to form higher order structures.

Subsequently, a catalog of building blocks was developed by Sallen and Key (3), which led to a much broader interest in active filters. This was due in no small part to removal of the need for classical synthesis expertise.

However, widespread use of active filters was still inhibited by concerns over sensitivity, particularly when compared to the passband performance of passive filters. This was overcome by the simulation of the floating inductor (4) and the widespread availability of operational amplifiers whose high-quality performance and low cost resulted in a fundamental change in design philosophy.

Designers, previously cost-constrained to single-amplifier second-order sections, were now able to consider multiamplifier sections whose performance and multipurpose functions made commercial production a viable proposition. In particular, the state variable topology (5) formed the basis for a universal filter yielding all basic filtering functions from a single structure.

Inductor replacement and direct simulation techniques such as the leapfrog approach (6) offered low-sensitivity analogs of classical LC filters. The difficulty in tuning these devices was simplified enormously by the introduction of computer-controlled laser trimming using hybrid microelectronics technology. Indeed, by the mid-1970s, sophisticated fifth-order elliptic characteristic filters were in large-scale production within the Bell System (7).

Thus, over a period of 20 years (1954–1974), active filter designers had come to rely upon a relatively small number of basic building blocks to form second-order sections, or were basing higher-order designs on analogs of LC structures. Although many realizations used discrete components, larger-scale production of thick and thin film hybrid microelectronic structures was quite common.

The advent of switched-capacitor filters in 1979 (8) overcame the need to laser trim resistors and yielded the first fully integrated active filters. While truly a sampled-data technique, the use of sufficiently high clock frequencies meant that active filters could be used up to 100 kHz, far higher than by conventional analog techniques. Subsequent developments have led to metal-oxide semiconductor field-effect transistor-capacitor (MOSFET-C) and operational transconductance amplifier-capacitor (OTA-C) filters (9) which yield authentic analog performance at frequencies exceeding 1 MHz.

The following sections will concentrate on a few fundamental filter design techniques that form the basis for modern active filter design. The Sallen and Key, multiple loop feedback, and state variable structures have stood the test of time and have proven to be as effective in discrete component realizations as they have in MOSFET-C structures. They all form higher-order filters when cascaded with similar sections. Finally, the leapfrog design and direct replacement techniques are discussed as examples of direct higher-order filter synthesis.

Table 1. Comparison of Active and Passive Filter Properties

Audio Band Filters	
LC	Active RC
Bulky	Small
Lossy (low Q)	Lossless (high Q)
Stable (absolutely)	Stability depends upon design
Transmission loss	Capable of transmission gain

SECOND-ORDER STRUCTURES

The fundamental building blocks for active RC filters are second-order structures which can readily be cascaded to realize higher-order approximating functions described by the general voltage transfer function:

$$\frac{V_o}{V_i} = H \cdot \frac{\left\{s^2 + \frac{\omega_z}{Q_z}s + \omega_z^2\right\}}{\left\{s^2 + \frac{\omega_p}{Q_p}s + \omega_p^2\right\}} \tag{1}$$

where ω_z, Q_z and ω_p, Q_p refer to the zero and pole frequency and Q, respectively. All-pole functions (low-pass, bandpass, high-pass) occur when only one of the numerator terms (s^0,

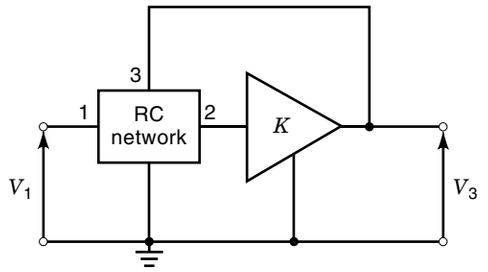

Figure 1. Sallen and Key structure consisting of a controlled source and an RC network. Appropriate choice of the RC network yields all basic forms of second-order transfer functions.

s^1, or s^2) is present. A notch occurs when the s^1 term disappears in the numerator. We will not discuss the more general case (10) that arises when all numerator terms are present simultaneously.

The topologies that follow are suitable for design using discrete, hybrid, or fully monolithic fabrication. Furthermore, they have stood the test of time for ease of design, tuning simplicity, and relatively low cost.

Sallen and Key

Sallen and Key originally proposed (3) a family of all-pole filters based upon the circuit shown in Fig. 1, for which

$$\frac{V_3}{V_1} = \frac{-Ky_{21}}{y_{22} + Ky_{23}} \tag{2}$$

By appropriate choice of the passive RC network, it is possible to realize all forms of basic filter. However, because the creation of a band-stop (notch) section requires the use of twin T networks, which are inherently difficult to tune, we confine our discussion to the realization of all-pole functions.

Table 2. Sallen and Key Realizations

Circuit No.	RC Structure	Voltage Transfer Function[a]
1	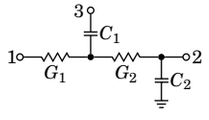	$\dfrac{\left(\dfrac{KG_1G_2}{C_1C_2}\right)}{s^2 + s\left\{\dfrac{G_2}{C_2} + \dfrac{G_1+G_2}{C_1} - \dfrac{KG_2}{C_2}\right\} + \dfrac{G_1G_2}{C_1C_2}}$
2	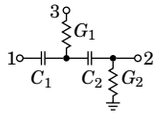	$\dfrac{Ks^2}{s^2 + s\left\{\dfrac{G_2}{C_2} + \dfrac{G_2}{C_1} + \dfrac{G_1}{C_1}(1-K)\right\} + \dfrac{G_1G_2}{C_1C_2}}$
3	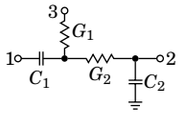	$\dfrac{s\left(\dfrac{KG_2}{C_2}\right)}{s^2 + s\left\{\dfrac{G_2}{C_2} + \dfrac{G_1+G_2}{C_1}\right\} + (1-K)\dfrac{G_1G_2}{C_1C_2}}$
4	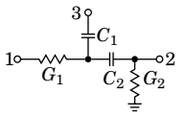	$\dfrac{s\left(\dfrac{KG_1}{(1-K)C_1}\right)}{s^2 + \dfrac{s}{(1-K)}\left\{\dfrac{G_1}{C_1} + \dfrac{G_2}{C_1} + \dfrac{G_2}{C_2}\right\} + \dfrac{G_1G_2}{(1-K)C_1C_2}}$

[a] $K > 0$ for circuits 1 and 2, $K < 0$ for circuits 3 and 4.

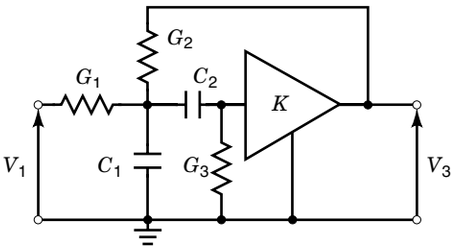

Figure 2. Sallen and Key second-order bandpass filter using positive-gain controlled source.

Table 2 illustrates four topologies and the resulting voltage transfer function when that RC structure is used in the circuit of Fig. 1. Thus, it is seen that low-pass and high-pass sections can be achieved with a positive-gain controlled source, whereas the two bandpass sections require a negative-gain controlled source (11).

Although not included in the original catalog, the five-element bandpass circuit of Fig. 2, which utilizes a positive-gain controlled source, is now generally incorporated under the Sallen and Key banner. In this case:

$$\frac{V_3}{V_1} = \frac{s\dfrac{KG_1}{C_1}}{s^2 + \left\{\dfrac{G_2(1-K)}{C_1} + \dfrac{(G_1+G_3)}{C_1} + \dfrac{G_3}{C_1}\right\}s + \dfrac{G_3(G_1+G_2)}{C_1C_2}} \tag{3}$$

Design is most commonly restricted to the positive-gain controlled source realizations, despite the inherent positive feedback used to enhance Q_p. In general, if realizations are restricted to $Q_p \leq 10$, the advantages of the lower component spread in this design outweigh the stability considerations. Design is relatively straightforward and proceeds by coefficient matching.

Example 1. For our example, we design a second-order low-pass Chebyshev filter having 0.5 dB passband ripple and a passband gain of 20 dB. From the standard tables (12–15), the normalized transfer function is

$$\frac{V_3}{V_1} = \frac{H}{s^2 + 1.426s + 1.516} \tag{4}$$

A passband gain of 20 dB is equivalent to an absolute gain of 10, so that $H = 15.16$. By matching the low-pass expression from Table 2 and the coefficients of Eq. (4), we obtain

$$\frac{KG_1G_2}{C_1C_2} = 15.16 \tag{5a}$$

$$\frac{G_1G_2}{C_1C_2} = 1.516 \tag{5b}$$

$$\frac{G_2}{C_2} + \frac{G_1+G_2}{C_1} - \frac{KG_2}{C_2} = 1.426 \tag{5c}$$

Thus, $K = 10$ [from Eqs. (5a) and (5c)]. The remaining two equations contain four unknowns, indicating freedom of choice for two of the elements. Such freedom of choice is a characteristic of the coefficient-matching technique. For convenience, set $C_1 = C_2 = IF$, since this is highly desirable in

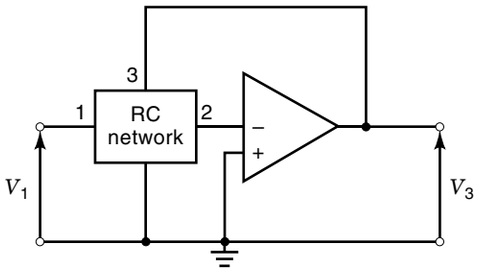

Figure 3. Multiple feedback (MFB) structure consisting of an operational amplifier and an RC network. Appropriate choice of the RC network yields all basic forms of second-order transfer functions.

many practical realizations. As a result,

$$G_1G_2 = 1.516 \tag{6a}$$

$$G_1 - 8G_2 = 1.426 \tag{6b}$$

The only solution yielding positive values is $G_1 = 4.268$ S and $G_2 = 0.355$ S. Impedance and frequency denormalization can be applied, depending upon specific design requirements.

Realization of the basic low-pass Sallen and Key filter has been widely discussed in the literature (11). Popular alternatives to the $C_1 = C_2 = IF$ used above are as follows:

1. Setting $C_1 = C_2 = C$, $G_1 = G_3 = G$, and $K = 3 - (1/Q)$
2. Setting $K = 1$ (thereby eliminating two gain-setting resistors), $G_1 = nG_3$ and $C_1 = mC_2$
3. Setting $K = 2$ (for equal-valued gain-setting resistors), $C_1 = C_2 = C$ and $G_3 = Q^2G_1$

Multiple Feedback Structure

The multiple feedback (MFB) structure (16) is derived from the general feedback configuration of Fig. 3, in which the active element is an ideal operational amplifier.

The most common realization of the RC network is shown in Fig. 4, which yields the MFB transfer function

$$\frac{V_3}{V_1} = \frac{-Y_1Y_3}{Y_5(Y_1 + Y_2 + Y_3 + Y_4) + Y_3Y_4} \tag{7}$$

The basic all-pole functions can be realized by single-element replacement of the admittances $Y_1 \rightarrow Y_5$, yielding a highly stable, negtive-feedback circuit. Specific realizations of the all-pole functions are shown in Table 3.

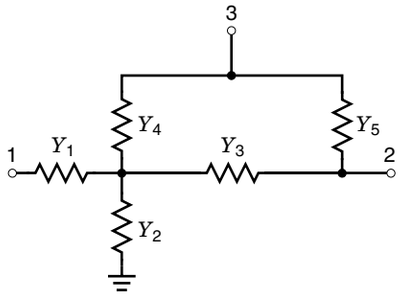

Figure 4. Three-terminal, double-ladder structure for use in MFB sections.

Table 3. MFB Structure and Voltage Transfer Functions

Filter Type	Network	Voltage Transfer Function
(*a*) Low-pass	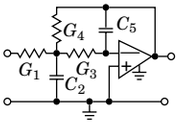	$\frac{-G_1G_3}{s^2C_2C_5 + sC_5(G_1 + G_3 + G_4) + G_3G_4}$
(*b*) High-pass	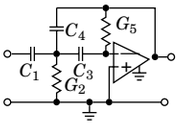	$\frac{-s^2C_1C_3}{s^2C_3C_4 + sG_5(C_1 + C_3 + C_4) + G_2G_5}$
(*c*) Bandpass	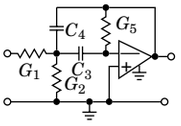	$\frac{-sG_1C_3}{s^2C_3C_4 + sG_5(C_3 + C_4) + G_5(G_1 + G_2)}$

As for Sallen and Key sections, design proceeds by coefficient matching. A widely used design set is illustrated in Table 4, for which both bandpass and high-pass circuits use equal-valued capacitors. No such solution is possible for the low-pass circuit, though an equal-valued resistor pair is possible.

Although highly stable, the MFB structure has a pole Q dependent upon the square root of component ratios. Thus, for a Q_p of n, the maximum component spread will be proportional to n^2. As a result, the MFB arrangement is best suited to modest values of Q_p, typically not greater than 10.

Modified Multiple-Loop Feedback Structure

In positive-feedback topologies such as the Sallen and Key, Q_p is enhanced by subtracting a term from the damping (s^1) coefficient in the denominator. By contrast, in negative-feedback topologies such as the MFB, high values of Q_p are obtained at the expense of large spreads in element values. The two techniques are combined in the modified multiple-loop

Table 4. Element Values for MFB Realizations (*H* is the Numerator Constant in Each Case)

Element Value		
Bandpass	High-pass	Low-pass
$G_1 = H$	$C_1 = H$	$G_1 = \frac{H}{\omega_p}$
$G_2 = 2\omega_pQ_p - H$	$G_2 = \omega_p(2 + H)Q_p$	$C_2 = \frac{Q_p(2\omega_p^2 + H)}{\omega_p^2}$
$C_3 = 1$	$C_3 = 1$	$G_3 = \omega_p$
$C_4 = C_3$	$C_4 = C_3$	$G_4 = G_3$
$G_5 = \frac{\omega_p}{2Q_p}$	$G_5 = \frac{\omega_p}{Q_p(2 + H)}$	$C_5 = \frac{\omega_p^2}{Q_p(2\omega_p^2 + H)}$

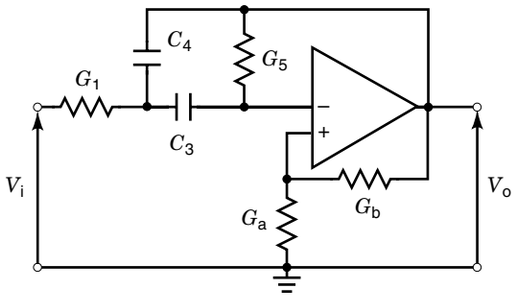

Figure 5. Modified multiple-loop feedback (MMFB) structure due to Deliyannis which yields a second-order bandpass function. By judicious use of positive feedback, this circuit reduces the large component spreads which are characteristic of the MFB structure while yielding greater stability margin than the Sallen and Key arrangement.

feedback (MMFB) circuit (17) of Fig. 5, for which

$$\frac{V_o}{V_i} = \frac{-sC_3G_1(1+k)}{s^2C_3C_4 + s\{G_5(C_3+C_4) - kC_3G_1\} + G_1G_5} \tag{8}$$

where $k = G_b/G_a$, and the Q-enhancement term signifies the presence of positive feedback.

Design of this bandpass circuit proceeds by coefficient matching, although the reader is advised to adopt the step-by-step procedure developed by Huelsman (11).

A generalization of the MMFB circuit, yielding a fully biquadratic transfer ratio has been developed by Friend et al. (18), as shown in Fig. 6. This arrangement was used extensively in the Bell System where the benefits of computer-controlled (deterministic) laser trimming techniques and large-scale manufacture were utilized. Although this resulted in quite exacting realizations using tantalum thin-film technology, the structure is less suited to discrete component realizations. An ordered design process based upon coefficient matching is presented elsewhere by Huelsman (15).

State Variable Structure

Based upon analog computer design techniques, the state variable (SV) structure (5) assumed popularity because of its versatility and ease of tuning. The advent of the operational amplifier eliminated earlier cost concerns, and the ability to realize relatively high-Q sections remains an attractive consideration. However, it is the ability of the circuit to yield all basic forms of second-order sections by appropriate choice of output terminal that has made it so popular for commercial manufacture (19). Custom filters are readily fabricated by appropriate interconnection of terminals, yielding the universal filter terminology of several vendors. In particular, highly reliable notch filters are possible through the addition of a summing amplifier to the basic three-amplifier array.

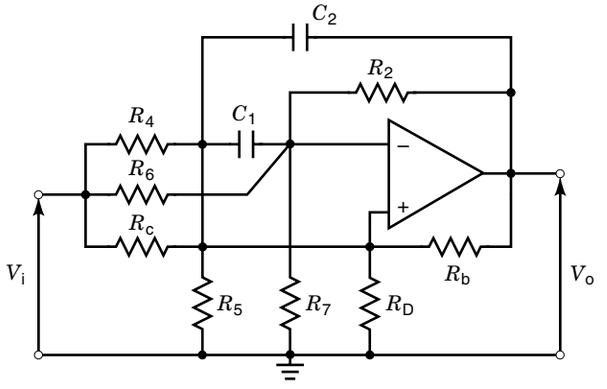

Figure 6. The Friend biquad which generalizes the MMFB structure of Fig. 5 so as to yield biquadratic filters.

The circuit shown in Fig. 7 is an example of a state-variable section and can be recognized as an analog computer realization of a second-order differential equation. It is more commonly referred to as the Huelsman-Kerwin-Newcomb (HKN) filter (5). In the frequency domain it is capable of yielding a variety of voltage transfer functions, according to the particular output connections used. Assuming ideal operational amplifiers, the specific transfer functions are as follows:

1. The *low-pass response* with

$$\frac{V_1}{V_i} = \left(\frac{R_2[R_3+R_{10}]}{R_3[R_1+R_2]}\right) \Big/ D(s) \tag{9a}$$

2. The *bandpass response* with

$$\frac{V_2}{V_i} = -R_9C_2s\left(\frac{R_2[R_3+R_{10}]}{R_3[R_1+R_2]}\right) \Big/ D(s) \tag{9b}$$

3. The *high-pass response* with

$$\frac{V_3}{V_i} = \frac{R_2(R_3+R_{10})}{R_3(R_1+R_2)}C_1C_2R_8R_9s^2 \Big/ D(s) \tag{9c}$$

where

$$D(s) = C_1C_2R_8R_9s^2 + \left\{\frac{R_1(R_3+R_{10})}{R_3(R_1+R_2)}\right\}C_2R_9s + \frac{R_{10}}{R_3}$$

A general biquadratic function may be obtained by combining the various outputs via a summing network, as shown in Fig. 8. The composite voltage transfer function then becomes

$$\frac{V_o}{V_i} = \frac{R_2(R_{10}+R_3)R_5(R_6+R_7)}{(R_1+R_2)R_3(R_4+R_5)R_7} \cdot \left\{\frac{C_1C_2R_8R_9s^2 + \left(\frac{[R_4+R_5]R_6}{R_5[R_6+R_7]}\right)R_9C_2s + \frac{R_4}{R_5}}{C_1C_2R_8R_9s^2 + \left(\frac{R_1[R_3+R_{10}]}{R_3[R_1+R_2]}\right)C_2R_9s + \frac{R_{10}}{R_3}}\right\} \tag{10}$$

Now consider the design of a low-pass response

$$T(s) = \frac{H}{s^2 + (\omega_p s/Q_p) + \omega_p^2} \tag{11}$$

It is clear from Eqs. 9(a) and (10) that there is considerable flexibility in the design since there are nine passive components and only three specified variables in Eq. (11).

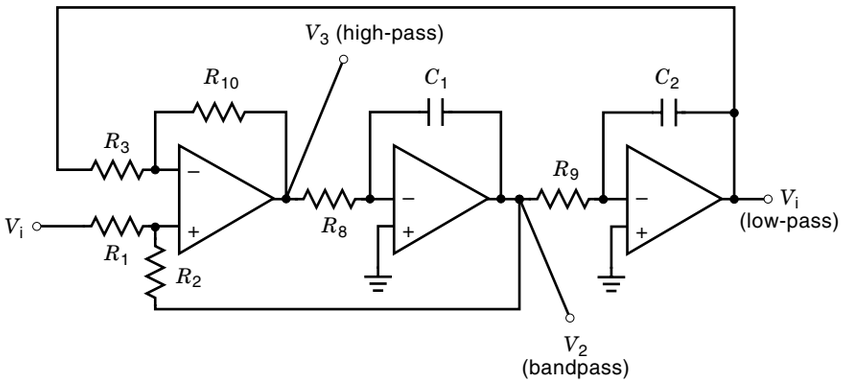

Figure 7. State variable filter capable of yielding a variety of all-pole second-order transfer functions.

The design equations are thus

$$\omega_p = \sqrt{\frac{R_{10}}{R_3 R_8 R_9 C_1 C_2}} \tag{12a}$$

$$Q_p = \frac{\sqrt{\dfrac{R_{10}}{R_3} \cdot C_1 C_2 R_8 R_9}}{\left\{\dfrac{R_1(R_3 + R_{10})}{R_3(R_1 + R_2)} \cdot R_9 C_2\right\}} \tag{12b}$$

$$H = \frac{R_2(R_3 + R_{10})}{R_3(R_1 + R_2) C_1 C_2 R_8 R_9} \tag{12c}$$

Selecting $C_1 = C_2 = C$ and $R_1 = R_3 = R_{10} = R$ gives

$$\omega_p = (R_8 R_9 C^2)^{-1/2} \tag{13a}$$

$$Q_p = \frac{(R + R_2)}{2R}\sqrt{\frac{R_8}{R_9}} \tag{13b}$$

$$H = \frac{2R_2}{(R + R_2) C^2 R_8 R_9} \tag{13c}$$

Setting $C = IF$ and $R_8 = R_9 = R'$ yields the following simplified equations

$$\omega_p^2 = \frac{1}{R'^2} \tag{14a}$$

$$Q_p = \frac{1}{2}\left(1 + \frac{R_2}{R}\right) \tag{14b}$$

$$H = \frac{2R_2/R}{\left(1 + \dfrac{R_2}{R}\right) R'^2} \tag{14c}$$

Therefore, the design equations are

$$R' = \frac{1}{\omega_p} \tag{15a}$$

$$\frac{R_2}{R} + 2Q_p - 1 \tag{15b}$$

The gain constant, H, is fixed as $[2 - (1/Q_p)]\omega_p^2$.

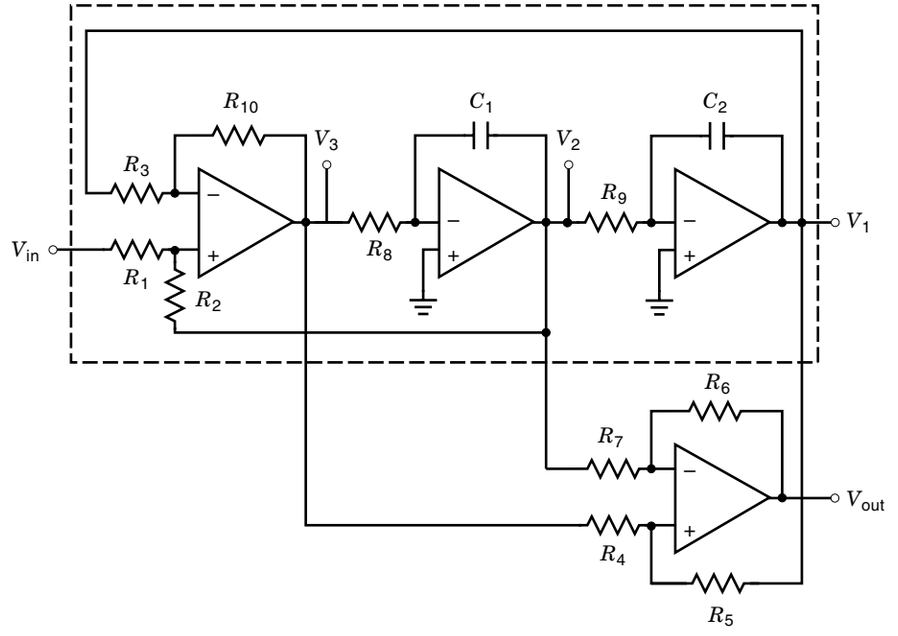

Figure 8. Composite state variable structure. The addition of an output summing network to the arrangement of Fig. 7 yields fully biquadratic transfer functions.

Example 2. Here we design a state-variable filter satisfying the following normalized elliptic function characteristic having a notch at 1.4 kHz.

$$T(s) = \frac{H(s^2 + \omega_z^2)}{s^2 + \frac{\omega_p}{Q_p}s + \omega_p^2} = \frac{s^2 + 1.438664}{s^2 + 0.314166s + 1.167222} \tag{16}$$

Thus, $\omega_z = 1.199$, $\omega_p = 1.08038$, and $Q_p = 3.4389$.

Realization requires the use of the summing network to combine the low-pass and high-pass outputs. Since no band-pass component is required, the left-hand end of resistor R_7 (Fig. 8) should be grounded.

Now consider the realization of the low-pass section. Set $R = C = 1$ and Eqs. 15(a) and (b) to give the normalized component values as

$$\begin{aligned} C_1 &= C_2 = 1F \\ R' &= R_8 = R_9 = 0.926\Omega \\ R &= 1\Omega \quad \text{so that } R_1 = R_3 = R_{10} = 1\Omega \\ &\quad \text{and } R_2 = 5.878\Omega \end{aligned}$$

The gain constant, H, has the value 1.995. The frequency denormalization factor, ω_n, is

$$\omega_n = \frac{2\pi \times 1.4 \times 10^3}{1.199} = 7.351 \times 10^3$$

Assume that available capacitors have a value of 6800 pF. Then, the impedance denormalization factor is evaluated as

$$Z_n = \frac{1}{6800 \times 10^{-12} \times 7.351 \times 10^3} = 20\ \text{k}\Omega$$

Therefore, the denormalized values are

$$\left.\begin{aligned} C_1 &= C_2 = 6800\ \text{pF} \\ R_1 &= R_3 = R_{10} = 20\ \text{k}\Omega \\ R_8 &= R_9 = 18.7\ \text{k}\Omega \\ R_2 &= 118\ \text{k}\Omega \end{aligned}\right\} \text{ standard 1\% values}$$

The high-pass and low-pass outputs may now be combined to yield the desired transfer function of Eq. (16). Thus, by substituting normalized element values into Eq. (10)

$$\frac{V_o}{V_{in}} = \frac{1.709R_5(R_6 + R_7)}{R_7(R_4 + R_5)} \left\{ \frac{s^2 + 1.1672(R_4/R_5)}{s^2 + 0.314179s + 1.1672} \right\} \tag{17}$$

The location of ω_z is obtained by appropriate choice of the resistor ratio, R_4/R_5. Hence,

$$\frac{R_4}{R_5} = 1.2326$$

Choosing $R_5 = 20\ \text{k}\Omega$ gives $R_4 = 24.65\ \text{k}\Omega$. The dc gain of the filter is determined by appropriate choice of R_6/R_7. If these resistors are set equal at 20 kΩ, the resulting dc gain is 5.52 dB.

The filter may be tuned by means of the R_4 to R_5 ratio to locate the notch accurately. In practice, this may be observed by closing a Lissajous pattern on an oscilloscope. The frequency at which this occurs will be ω_z.

HIGHER-ORDER REALIZATIONS

Higher-order filters may be designed by cascading second-order structures of the form described in the previous section. Odd-order functions are accommodated by the addition of a single-pole section or, if combined with a low-Q pole-pair, by the addition of a third-order section. The section types (Sallen and Key, MFB, MMFB, SV) may be mixed in a realization so that the SV is used for higher Q and notch functions. Particular care must be taken with the selection of pole-zero pairs and the ordering of sections due to considerations of dynamic range. A fuller discussion of these features is described elsewhere (20–22).

The major advantage of the cascade approach is the ability to independently tune each pole pair. This is offset to some degree by the higher sensitivity to component changes and the care needed to properly order the sections and pair the poles and zeroes. A widely used alternative bases designs on the passive LC prototype whose passband sensitivity is minimal. The most common approaches are described below.

Inductor Replacement

As indicated above, it is highly desirable to base active RC filter designs upon passive LC prototypes because of the resulting low passband sensitivity. An added advantage results from the availability of tabulated LC designs (12–15), which obviate the need for sophisticated synthesis techniques. Thus, for a given standard approximating function, the LC prototype may be established with the aid of design tables.

The resulting inductors may be replaced by means of an appropriately terminated generalized impedance converter (GIC). The ideal GIC is shown in Fig. 9, for which

$$Z_{11} = \frac{a_{11}}{a_{22}} = k(s)Z_L \tag{18a}$$

$$Z_{22} = \frac{a_{22}}{a_{11}} = \frac{1}{k(s)}Z_L \tag{18b}$$

if $a_{12} = a_{21} = 0$.

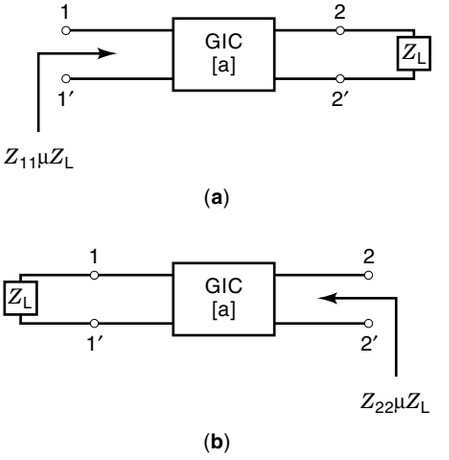

Figure 9. Generalized impedance converter (GIC). (a) Load at terminal 2. (b) Load at terminal 1.

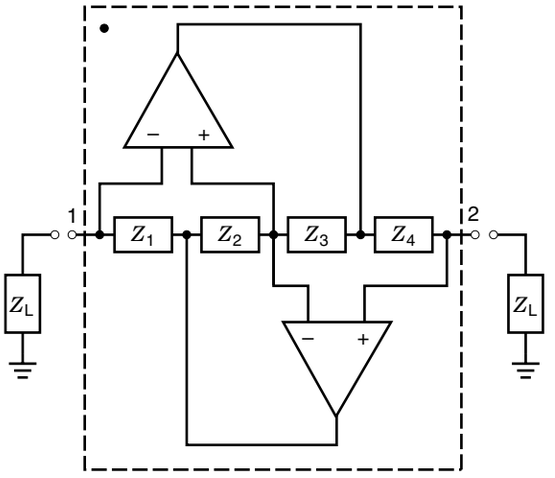

Figure 10. Antoniou GIC—the most widely used realization of this important circuit element.

The most commonly used realization of the GIC, from Antoniou (23), is shown in Fig. 10. In this case

$$k(s) = \frac{Z_1 Z_3}{Z_2 Z_4} \tag{19}$$

Thus, if we select

$$Z_1 = Z_3 = Z_4 = R \quad \text{and} \quad Z_2 = \frac{1}{sC}$$

we obtain $k(s) = sk'$. If $Z_L = R_1$, then

$$Z_{11} = sk'R_1$$

and we have simulated a grounded inductor whose Q value far exceeds that of a conventional coil. Indeed, audio band Q factors of the order of 1000 are readily obtained if high-quality capacitors are used in the GIC.

Grounded inductor simulation is readily applicable to the realization of high-pass filters, as illustrated in Fig. 11. Note that a dot (•) is used to denote terminal 1 of the GIC, because it is a directional device having a conversion factor $k(s)$ from terminal 1, and $1/k(s)$ from terminal 2.

The simulation of a floating inductor requires the use of two GICs, as shown in Fig. 12. However, the simulation of structures containing several floating inductors can become undesirable due to the excessive number of active blocks.

Frequency-dependent Negative Resistance

Depending upon the choice of impedances $Z_1 \rightarrow Z_4$, the GIC of Fig. 10 may be used to provide conversion factors of s^n, where $n = \pm 1, \pm 2$. If one internal port impedance is capacitive and the other three are resistive, the conversion factor is $k's$ in one direction and $1/k's$ in the other. Use of two internal capacitors yields $k''s^2$ and $1/k''s^2$, respectively. Using the first combination of elements and a capacitor at port 1 produces a port 2 impedance given by $Z_{22} = (1/s^2)D$, where D is frequency invariant. At real frequencies, this represents a second-order

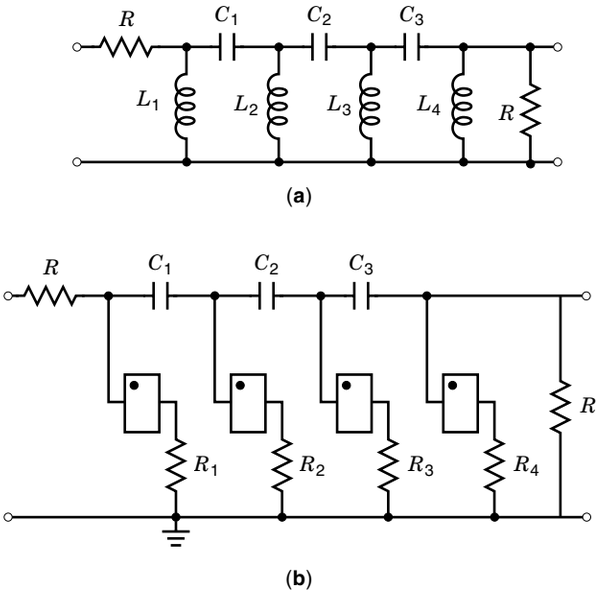

Figure 11. High-pass filter realization using direct inductor replacement. (a) Passive prototype. (b) Active realization using resistor-terminated GICs to realize the grounded inductors.

capacitor, because

$$Z_{22}\Big|_{s=j\omega} = \frac{-1}{\omega^2 D} \tag{20}$$

However, the term *frequency-dependent negative resistance* (FDNR) has achieved universal adoption. D is in units of (farad)^2·ohms and is represented by the symbol shown in Fig. 13.

A synthesis technique incorporating FDNRs (24) overcomes the need for floating inductor simulation in LC prototypes. If the admittances in a network are scaled by a factor s, neither the voltage nor current transfer ratios are affected, because they are formed from ratios of impedance or admittance parameters. However, scaling does affect the network elements as follows:

Admittance $Y(s)$ becomes $sY(s)$ (transformed admittance)
Capacitor sC becomes s^2C (FDNR)
Inductor $1/sL$ becomes $1/L$ (resistor)
Resistor $1/R$ becomes s/R (capacitor)

Inductors are thus eliminated and a new, but topologically equivalent, network is formed.

Example 3. In this example, we realize a doubly terminated low-pass filter having a fourth-order Butterworth characteris-

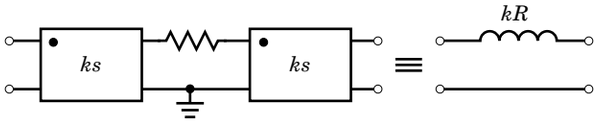

Figure 12. GIC realization of a floating inductor.

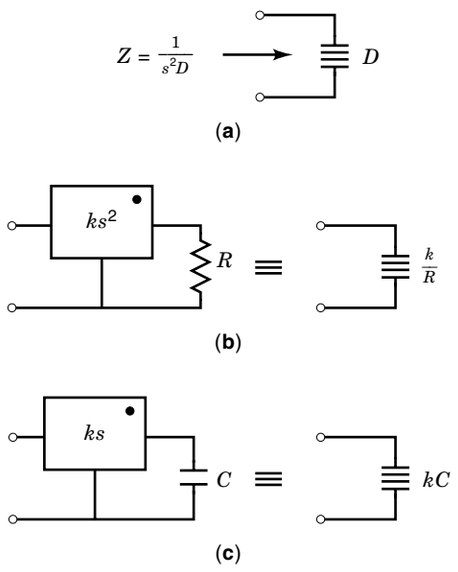

Figure 13. FDNR symbol and realization. (a) Symbol for FDNR of value D. (b) Realization of FDNR by resistively-terminated GIC. (c) Realization of FDNR by capacitively-terminated GIC.

tic. From design tables, we obtain the LC prototype of Fig. 14(a). Transformation yields the so-called DCR network of Fig. 14(b). If biasing problems are encountered due to the presence of floating capacitors, they may be overcome by the addition of shunt resistors, R_A and R_B, as shown in Fig. 14(c). In order to preserve the passband loss of the original network, these resistors are arranged to yield a dc gain of 0.5. Hence,

$$\frac{R_B}{R_A + 0.7654 + 1.8478} = 0.5$$

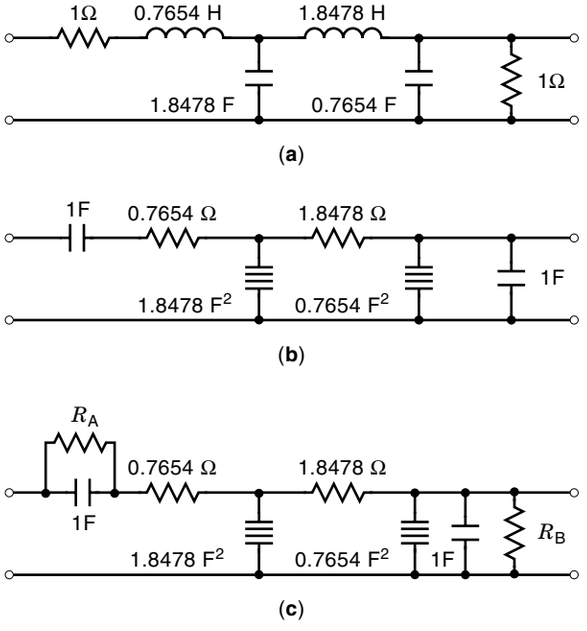

Figure 14. FDNR realization of low-pass filter. (a) LC prototype of fourth-order Butterworth filter. (b) DCR network derived from (a). (c) Resistive shunts added for biasing purposes.

for which, for example, R_A may be set at 100 Ω so as to avoid loading the capacitor.

Denormalization of the circuit is straightforward, noting that an FDNR of normalized value D_n, is denormalized using the expression

$$D = \frac{D_n}{Z_n \omega_n^2} \tag{21}$$

The FDNR approach is most effective when all inductors are floating. In more complex arrangements, floating FDNRs result whenever a floating capacitor is present in the original prototype. Since the replacement of each floating FDNR requires the use of two GICs, the alternative of partial transformation (25,26) is preferred.

The technique is illustrated in Fig. 15, for which the composite transmission matrix $[a']$ for the three-section cascade is given as

$$[a'] = \begin{bmatrix} 1 & 1 \\ 0 & \dfrac{1}{k_1 s^n} \end{bmatrix} \begin{bmatrix} a_{11} & \dfrac{a_{12}}{k_1 s^n} \\ k_1 a_{21} s^n & a_{22} \end{bmatrix} \begin{bmatrix} 1 & 0 \\ 0 & k_2 s^n \end{bmatrix} = \begin{bmatrix} a_{11} & \dfrac{a_{12} k_2}{k_1} \\ a_{21} & \dfrac{a_{22} k_2}{k_1} \end{bmatrix} \tag{22}$$

Hence, for matched GICs ($k_1 = k_2$), we see that $[a'] = [a]$.

The technique is illustrated in Fig. 16(a)–(c) for a bandpass section. Using direct FDNR realization of Fig. 16(b) would require a total of five GICs. The partial transformation of Fig. 16(c) reduces the requirement to three GICs. Clearly, the savings are more dramatic for higher-order realizations.

Leapfrog Realization

The leapfrog technique (6) was introduced over 40 years ago and represents the first of several multiloop feedback simulation methods (27–29). Its simplicity and elegance derives from a one-to-one relationship between passive reactances in a ladder structure and integrators in the leapfrog model.

The technique is particularly well suited to the realization of low-pass responses, which are the most difficult to realize by direct replacement methods. Although the presence of multiple feedback loops can render tuning difficult, the close matching of capacitor ratios and the similarity of the active blocks rendered this approach ideal for the realization of switched-capacitor filters (SCF). Indeed, SCF technology revitalized interest in the leapfrog approach.

Consider the output sections of the low-pass LC filter of Fig. 17(a). The relationships between the various voltages and currents are shown in Eqs. 23

$$i_1 = sC_1 R V_0 \tag{23a}$$
$$i_2 = i_1 + i_0 \tag{23b}$$
$$V_2 = \frac{sL_1}{R} i_2 \tag{23c}$$
$$V_3 = V_2 + V_0 \tag{23d}$$
$$i_3 = sC_2 R V_3 \tag{23e}$$
$$i_4 = i_3 + i_2 \tag{23f}$$
$$V_4 = \frac{sL_2}{R} i_4 \tag{23g}$$
$$V_5 = V_4 + V_3 \tag{23h}$$

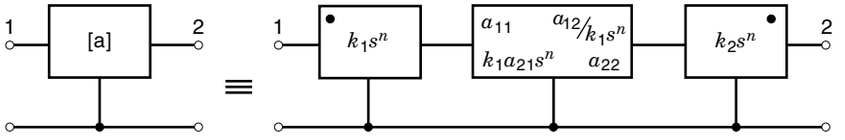

Figure 15. The use of two GICs to yield an embedded network equivalence which eliminates the need to realize floating FDNRs.

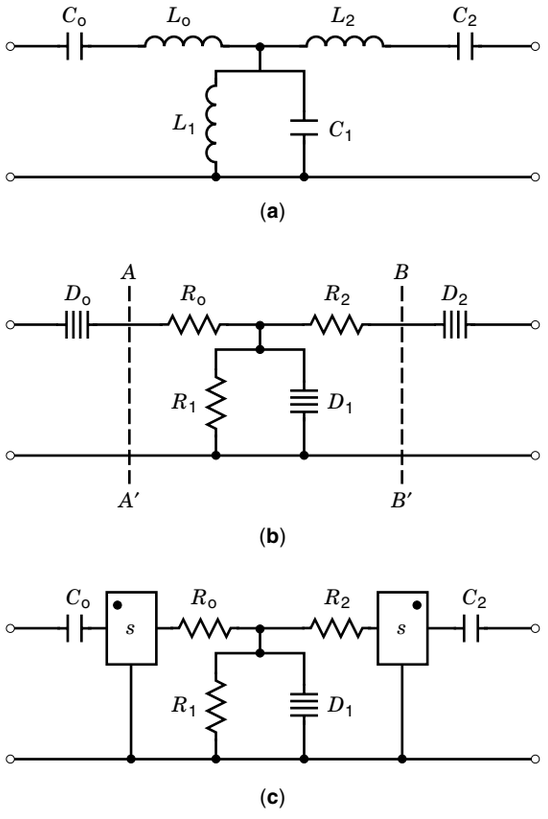

Figure 16. Partial transformation to eliminate floating FDNRs. (a) LC bandpass section. (b) DCR realization of (a). (c) Partial transformation of (a) by embedding the section $AA'BB'$ between two GICs.

Thus, working from output to input, we have alternating processes of differentiation and addition. Now, consider the multifeedback integrator structure of Fig. 17(b), for which

$$\theta_1 = sT_1\theta_0 \tag{24a}$$
$$\theta_2 = \theta_1 + \theta_0 \tag{24b}$$
$$\theta_3 = sT_2\theta_2 \tag{24c}$$
$$\theta_4 = \theta_3 + \theta_0 \tag{24d}$$
$$\theta_5 = sT_3\theta_4 \tag{24e}$$
$$\theta_6 = \theta_5 + \theta_4 \tag{24f}$$
$$\theta_7 = sT_4\theta_6 \tag{24g}$$
$$\theta_8 = \theta_7 + \theta_6 \tag{24h}$$

Thus, for every current and voltage in Eqs. (23a–h), there is a corresponding quantity θ_i in Eqs. (24a–h). Furthermore, if corresponding factors such as C_1R_1 and T_1, L_1/R and T_2 are set equal, the two systems have full equivalence.

As a result, LC low-pass structures may be simulated by a straightforward process, as illustrated in Fig. 18. More detailed discussions of this approach, including its extension beyond the low pass are presented elsewhere (14, Ch. 10). As an analog of a passive LC filter, the leapfrog structure provides a low sensitivity structure, and one which is inherently stable.

INTEGRATED FILTERS

As indicated previously, the earliest active filters were fabricated using discrete components and, eventually, operational amplifiers. The selection of high-quality capacitors and low-tolerance, high-performance resistors is crucial to the ultimate quality of the filter (20). Finally, the circuit must be tuned by the adjustment of one or more trimmer pots.

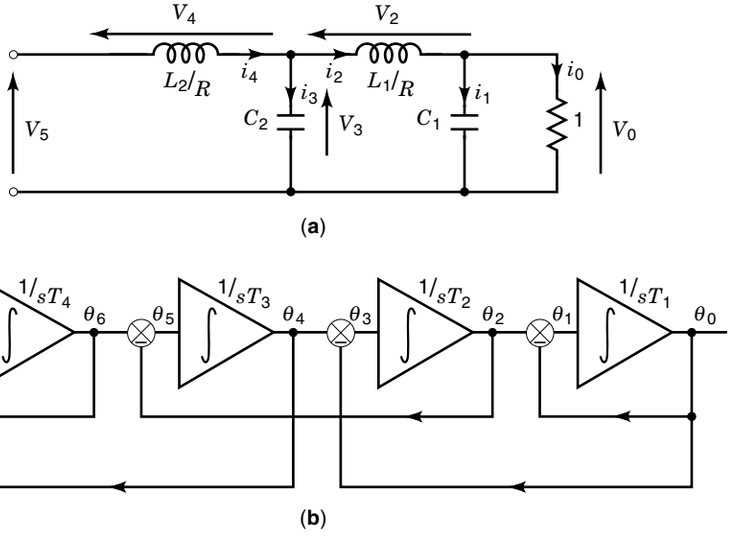

Figure 17. Basic equivalence of LC and leapfrog structures. (a) LC prototype. (b) Multifeedback integrator structure.

The advent of laser trimming, combined with thick and thin film hybrid microelectronic processing, not only led to larger-scale production but allowed for much more precise adjustment of resistors. Coupled with numerically controlled resistor adjustment, hybrid microelectronics fabrication led to more widespread use of active filters. However, the quest for ever-smaller structures, and for higher cut-off frequencies ultimately led to fully integrated filters. Several major technical problems inhibited the fabrication of fully integrated filters:

1. The relatively low bulk resistance of silicon, which meant that large values of resistance required an unduly large volume.
2. The relatively low dielectric constant of silicon which resulted in excessively large capacitor plate area.
3. The inability to trim passive elements.

Active-R filters (30–31) which utilize the single-pole roll-off model of an operational amplifier provide an effective capacitance for simple, high cut-off filters. However, the need to accurately determine the roll-off properties of each amplifier renders this approach inefficient in the absence of sophisticated on-chip self-tuning circuitry (9).

Switched-capacitor filters were the first fully-integrated structures. Although they are strictly sampled-data systems, they simulate an analog system if the clock frequency is much higher than the cut-off frequency. Although a more detailed description of SCFs is presented in SWITCHED CAPACITOR NETWORKS, two of their advantages are worthy of note at this time:

1. The filters are fully integrated.
2. Performance depends upon the ratio of relatively small capacitors and an accurate clock to establish circuit time constants with high precision.

Fully integrated filters have been developed using the MOSFET-C (32) technique, which is based upon monolithic operational amplifiers, capacitors, and MOS (metal oxide semiconductor) transistors. The latter are biased in their ohmic region to yield tunable resistors. The technique allows the designer to take advantage of well-tried RC active filter design methods but is restricted in frequency by the operational amplifiers and the nonlinear nature of the simulated resistance.

Further limitations occur due to integrated circuit parasitics and switching noise resulting from the tuning circuitry. These problems can be overcome by using fully balanced differential circuits so that parasitic effects appear as common mode signals. Fully balanced circuits are usually derived from their single-ended counterparts, and are based upon well-tried structures such as those described in earlier sections. A useful general rule (9) for converting from single-ended to a balanced circuit is presented below:

- Identify ground node(s) in the single-ended circuit.
- Mirror the circuit at ground, duplicating all elements, and divide the gain of all active devices by two.
- Change the sign of the gain of all mirrored active devices and merge so that any resulting pair with inverting-noninverting gains becomes one balanced differential input-differential output device.
- Realize any devices whose sole effect in the original circuit is a sign inversion by a simple crossing of wires.

The conversion process for a state variable filter is shown in Fig. 19(a–b), while Fig. 19(c) shows the MOSFET-C realization in which the resistors of Fig. 19(b) have been replaced by MOSFET-simulated resistors.

By contrast, fully integrated active filters based upon the operational transconductance amplifier (OTA) (33–34) are

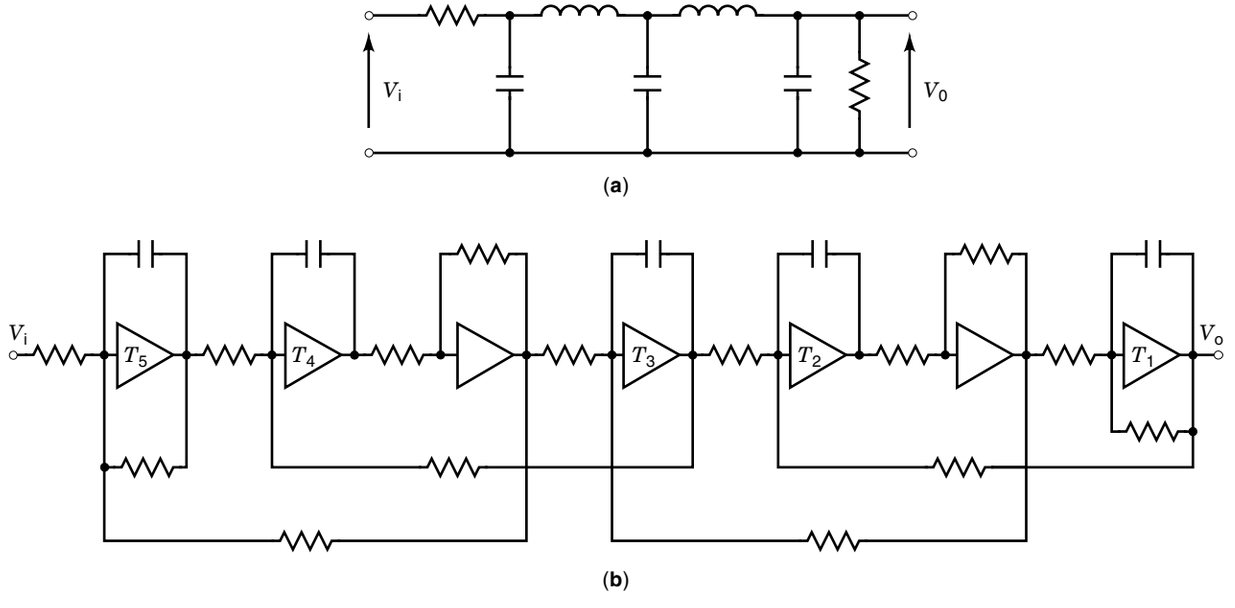

Figure 18. Leapfrog realization of low-pass LC filter. (a) Fifth-order LC filter. (b) Leapfrog realization of (a).

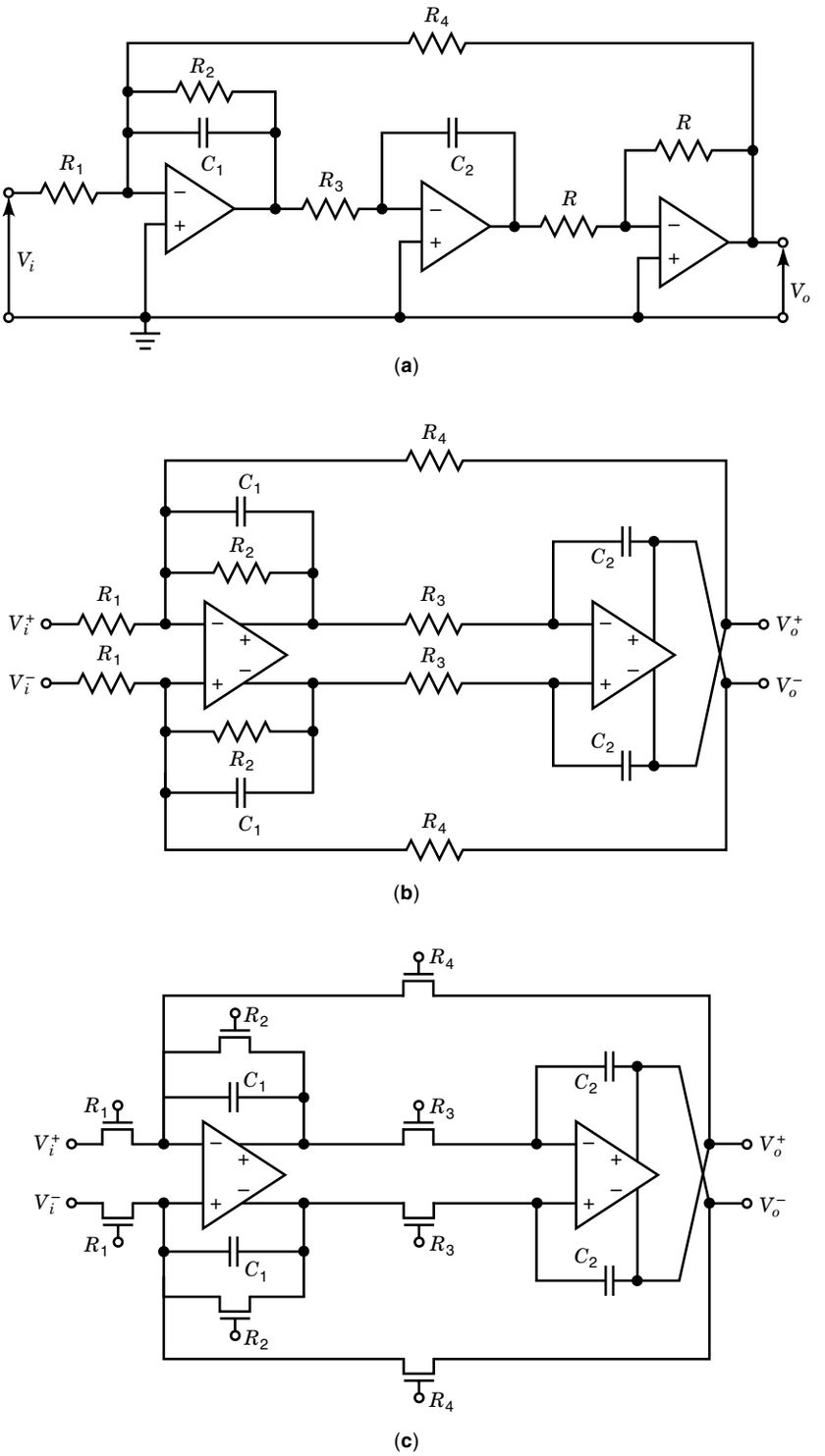

Figure 19. Realization of MOSFET-C state variable filter. (a) Original active RC version using single-ended amplifiers. (b) Fully differential, active-RC version. (c) MOSFET-C version with MOSFETs $R_1 \ldots R_4$ replacing equivalent resistors of (b).

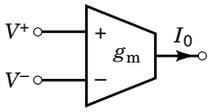

Figure 20. Circuit symbol for the operational transconductance amplifier (OTA).

simpler to design and have a much wider frequency range. This has led to OTA-C structures capable of accurate operation at frequencies beyond 100 MHz (35).

The OTA is a high-gain voltage-controlled current source, which is relatively easy to fabricate using CMOS or complementary bipolar technology. Some basic properties of the OTA are as follows:

1. High gain-bandwidth product that yields filters with higher operating frequencies than those using conventional operational amplifiers.
2. Can be electronically tuned to modify its transconductance.
3. Infinite input impedance and infinite output impedance.

The circuit symbol for the OTA is shown in Fig. 20, for which

$$I_0 = g_m(V^+ - V^-) \tag{25}$$

where g_m is the transconductance, a typical value being 500 μA/V. g_m can be controlled by Ic such that:

$$g_m = KIc \tag{26}$$

where Ic is in microamps and a typical value of K is 15. Of particular importance, Eq. (26) is valid over a wide range, perhaps as much as six decades for Ic, that is, 0.001 to 1000 μA. In addition, the gain-bandwidth is also proportional to Ic and may extend to hundreds of megahertz. This will be limited by input and output parasitics.

An OTA-C filter structure depends upon the ability of the OTA to simulate large values of resistance. Hence, in conjunction with relatively small values of capacitance, it is possible to set the appropriate filter time constants without undue use of silicon real estate.

Resistance can be simulated by the circuits shown in Figs. 21(a,b). For the grounded resistance,

$$-I_1 = I_0 = g_m(0 - V^-) = -g_m V_1$$

Hence,

$$R_{eq} = \frac{V_1}{I_1} = \frac{1}{g_m} \tag{27}$$

Thus, if $g_m = 10^{-5}S$, $R_{eq} = 100$ kΩ.

For the floating resistance of Fig. 21(b):

$$I_1 = -g_{m1}(V_2 - V_1) \tag{28a}$$

$$I_2 = -g_{m2}(V_1 - V_2) \tag{28b}$$

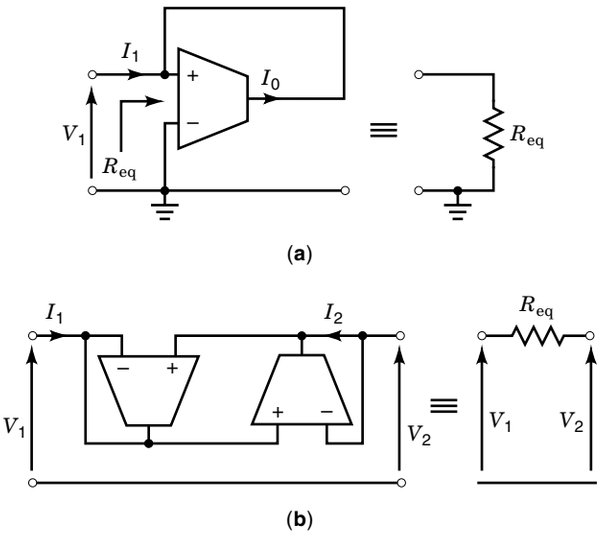

Figure 21. Resistance simulation using OTAs. (a) Grounded resistor. (b) Floating resistor.

from which:

$$\begin{bmatrix} I_1 \\ I_2 \end{bmatrix} = \begin{bmatrix} g_{m1} & -g_{m1} \\ -g_{m2} & g_{m2} \end{bmatrix} \begin{bmatrix} V_1 \\ V_2 \end{bmatrix} \tag{29}$$

For matched devices, $g_{m1} = g_{m2}$, and Eq. (29) represents a floating resistor of value $1/g_m$. Various building blocks can now be developed, forming the basis for simulation of structures such as the state variable. For example, the simple summer shown in Fig. 22(a) yields

$$V_0 = \frac{g_{m1}}{g_{m3}}V_1 + \frac{g_{m2}}{g_{m3}}V_2 \tag{30}$$

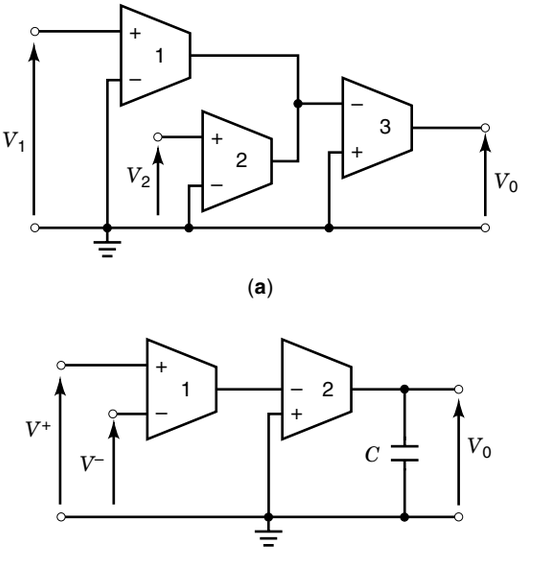

Figure 22. OTA filter building blocks. (a) Summer. (b) Damped integrator.

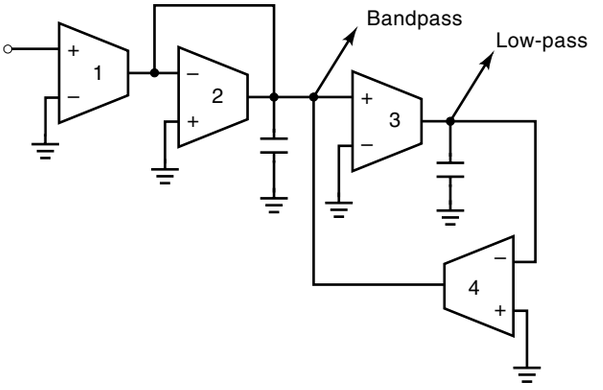

Figure 23. OTA circuit yielding both bandpass and low-pass second-order transfer functions.

whereas the circuit of Fig. 22(b) realizes a damped integrator, for which

$$V_0 = \frac{g_{m1}}{sC + g_{m2}}(V^+ - V^-) \tag{31}$$

Furthermore, by setting $g_{m2} = 0$ (eliminating the second OTA), Eq. (31) reduces to that of an undamped integrator.

Other biquads, not based directly on earlier topologies, may also be realized. For example, the biquad of Fig. 23 may be analyzed to yield a bandpass output of

$$\frac{V_{bp}}{V_i} = \frac{s(g_{m1}/C_1)}{s^2 + \left(\frac{g_{m2}}{C_2}\right)s + \frac{g_{m3}g_{m4}}{C_1C_2}} \tag{32}$$

SUMMARY

RC active filters have reached a degree of maturity that could not have been envisaged when they were first conceived over 40 years ago. The successive introductions of operational amplifiers, laser trimming, hybrid microelectronic fabrication, and, finally, fully integrated filters have all helped advance the state of the art. However, the thread linking all of these technological advances has been the retention of a small number of topologies and techniques that have been proven to yield reliable filters for large-scale practical applications. These structures have formed the basis for discussion in this article. By no means do they represent all the possibilities, but they do form a solid basis upon which further study may be based.

BIBLIOGRAPHY

1. F. Jay (ed.), *IEEE Standard Dictionary of Electrical and Electronic Terms,* 4th ed., New York: IEEE Press, 1988.
2. J. G. Linvill, RC active filters, *Proc. IRE,* **12**: 555–564, 1954.
3. R. P. Sallen and E. L. Key, A practical method of designing RC active filters, *IRE Trans.,* **CT-2**: 74–85, 1955.
4. A. G. J. Holt and J. R. Taylor, Method of replacing ungrounded inductances by grounded gyrators, *Electron. Lett.,* **1** (4): 105, 1965.
5. W. J. Kerwin, L. P. Huelsman, and R. W. Newcomb, State-variable synthesis for insensitive integrated circuit transfer functions, *IEEE Journal,* **SC-2**: 87–92, 1967.
6. F. E. Girling and E. F. Good, Active filters, *Wireless World,* **76**: 341–345, 445–450, 1970. The leapfrog method was first described by the same authors in RRE Memo No. 1177, September, 1955.
7. R. A. Friedenson et al., RC active filters for the D3 channel bank filter, *Bell Syst. Tech. J.,* **54** (3): 507–529, 1975.
8. R. W. Brodersen, P. R. Gray, and D. A. Hodges, MOS switched-capacitor filters, *Proc. IEEE,* **67**: 61–75, 1979.
9. R. Schaumann, M. S. Ghausi, and K. R. Laker, *Design of Analog Filters,* Englewood Cliffs, NJ: Prentice-Hall, 1990.
10. R. W. Daniels, Approximation Methods for Electronic Filter Design, New York: McGraw-Hill, 1974.
11. P. Bowron and F. W. Stephenson, *Active Filters for Communications and Instrumentation,* London: McGraw-Hill, 1979.
12. A. I. Zverev, *Handbook of Filter Synthesis,* New York: Wiley, 1967.
13. E. Christian and E. Eisenman, *Filter Design Tables and Graphs,* New York: Wiley, 1966.
14. F. W. Stephenson (ed.), *RC Active Filter Design Handbook,* New York: Wiley, 1985.
15. L. P. Huelsman, *Active and Passive Analog Filter Design—An Introduction,* New York: McGraw-Hill, 1993.
16. F. W. Stephenson, Single-amplifier multiple-feedback filters, in W-K. Chen, (ed.), *The Circuits and Filters Handbook,* New York: CRC Press/IEEE Press, 1995.
17. T. Deliyannis, High-Q factor circuit with reduced sensitivity, *Electron. Lett.,* **4** (26): 577–579, 1968.
18. J. J. Friend, C. A. Harris, and D. Hilberman, STAR: an active biquadratic filter section, *IEEE Trans. Circuits Syst.,* **CAS-22**: 115–121, 1975.
19. L. P. Huelsman and P. E. Allen, *Introduction to the Theory and Design of Active Filters,* New York: McGraw-Hill, 1980.
20. F. W. Stephenson and W. B. Kuhn, Higher-order filters, in J. T. Taylor and Q. Huang (eds.), *CRC Handbook of Electrical Filters,* New York: CRC Press, 1997, pp. 119–139.
21. G. S. Moschytz, A second-order pole-zero pair selection for nth-order minimum sensitivity networks, *IEEE Trans.,* **CT-17** (4): 527–534, 1970.
22. M. S. Ghausi and K. R. Laker, *Modern Filter Design,* Englewood Cliffs, NJ: Prentice-Hall, 1981.
23. A. Antoniou, Realization of gyrators using operational amplifiers and their use in RC-active network synthesis, *Proc. IEEE,* **116** (11): 1838–1850, 1969.
24. L. T. Bruton, Network transfer functions using the concept of frequency-dependent negative resistance, *IEEE Trans.,* **CT-16**: 406–408, 1969.
25. A. W. Keen and J. L. Glover, Active RC equivalents of RCL networks by similarity transformation, *Electron. Lett.* **7** (11): 288–290, 1971.
26. L. T. Bruton and A. B. Haase, Sensitivity of generalized immittance converter-embedded ladder structures, *IEEE Trans.,* **CAS-21** (2): 245–250, 1974.
27. G. Hurtig, The primary resonator block technique of filter synthesis, *Proc. IEEE International Filter Symposium,* Santa Monica, CA, April 1972, p. 84, [US Patent 3,720,881, March, 1973].
28. K. R. Laker and M. S. Ghausi, Synthesis of low-sensitivity multiloop feedback active RC filter, *IEEE Trans.,* **CAS-21** (2): 252–259, 1974.
29. J. Tow, Design and evaluation of shifted-companion form of active filters, *Bell Syst. Tech. J.,* **54** (3): 545–568, 1975.
30. J. R. Brand and R. Schaumann, Active R filters: Review of theory and practice, *IEEE J.,* **ECS-2** (4): 89–101, 1978.

31. A. S. Sedra and P. O. Brackett, *Filter Theory and Design: Active and Passive,* Portland OR: Matrix, 1978.
32. Y. Tsividis, M. Banu, and J. Khoury, Continuous-Time MOSFET-C Filters in VLSI, *IEEE Trans.,* **CAS-33**: 1125–40, 1986.
33. Y. P. Tsividis and J. O. Voorman (eds.), *Integrated Continuous-Time Filters,* Piscataway, NJ: IEEE Press, 1993.
34. R. L. Geiger and E. Sanchez-Sinencio, Active filter design using operational transconductance amplifiers: A tutorial, *IEEE Circ. Dev. Mag.,* **CDM-1**: 20–32, 1985.
35. M. Atarodi and J. Choma, Jr., A 7.2 GHz bipolar operational transconductance amplifier for fully integrated OTA-C filters, *J. Analog Integ. Circ. Signal Process.,* **6** (3): 243–253, 1994.

F. WILLIAM STEPHENSON
Virginia Polytechnic Institute and
State University

ACTIVE FILTERS. See ANALOG FILTERS; CASCADE NETWORKS.

ACTIVE NETWORK SYNTHESIS. See CURRENT CONVEYORS.